BOREAL ENVIRONMENT RESEARCH 31: 125–145
ISSN 1797-2469 (online)
© 2026
Helsinki 17 January 2026

Atmospheric ducts in the Baltic Sea region 1940–2025

Lars Norin

Swedish Defence Research Agency, Box 1165, 58111 Linköping, Sweden
corresponding author's e-mail: lars.norin@foi.se

Received 15 May 2026, final version received 6 Oct. 2026, accepted 9 Oct. 2026

Norin L. 2026: Atmospheric ducts in the Baltic Sea region 1940–2025. *Boreal Env. Res.* 31: 125–145.

Variations in atmospheric refractivity impact how electromagnetic signals propagate over the sea, extending or limiting the range of communication and radar systems. Atmospheric ducts — layers in the atmosphere that act as waveguides — can substantially alter communication and radar ranges. This study presents a long-term climatology of atmospheric ducts across the Baltic Sea region using 86 years of ERA5 data (1940–2025). Duct occurrence shows strong seasonal and regional variability, with surface ducts frequently occurring in southern areas during summer while much less common in the north. In recent years, surface-duct occurrence has increased during spring, consistent with an earlier seasonal development of ducting conditions. These findings enhance understanding of when and where in the Baltic Sea region anomalous propagation is most likely to occur.

Introduction

The Baltic Sea region is one of the world's busiest maritime shipping zones (HELCOM 2010) and has recently also emerged as a geopolitical focal point (Crowther 2023, Swistek and Paul 2023, Haldén 2025). In such densely trafficked and militarily sensitive waters, electromagnetic signals are essential for both civilian and defense operations, supporting communication, navigation, and situational awareness. The effective range of these signals, particularly for near-surface applications, is strongly affected by atmospheric conditions. Spatial and temporal variations in the atmospheric refractive index influence propagation paths and, consequently, the performance of near-surface emitters such as radars or communication systems which can have significant real-world consequences. For example, it has been suggested that anomalous propagation conditions allowed for the targeting and subsequent sinking of the Russian warship *Moskva* in the Black Sea in April 2022 (Norin *et al.* 2023). A comprehensive understanding of the variability in the atmospheric refractive index across the Baltic Sea region is therefore warranted.

The influence of the atmospheric refractive index on electromagnetic signal propagation has been studied for nearly a century (see, e.g., Bean and Dutton 1968, Kerr 1987). Atmospheric ducts, i.e. layers where strong vertical gradients in the refractive index trap and guide electromagnetic waves, are prominent examples of such effects. Although the underlying mechanisms and physics of duct formation are well established, few studies have explored the spatial and temporal variability of ducting conditions in the Baltic Sea region (Norin 2023, Rautiainen *et al.* 2025).

The atmospheric refractive index can be measured *in situ* using, for example, masts (Grábner and Kvičera 2003, Falodun and Ajewole 2006), radiosondes (Steiner and Smith 2002,

Editor in charge of this article: Antti Arola
https://doi.org/10.60910/ber2026.5tkp-4036

Alappattu *et al.* 2016, Huang *et al.* 2022), or drones (Østenstad and Meltzer 2023, Hou *et al.*, 2024). While *in situ* measurements provide direct, high-temporal-resolution observations of the refractive index, they are inherently limited in spatial coverage. Even meteorological radiosondes, which are typically launched twice per day, are released from a limited number of (mostly land-based) sites.

To complement such sparse *in situ* observations, indirect methods infer atmospheric refractivity from changes in signal propagation under varying atmospheric conditions. Signals propagating at low elevation angles over sea surfaces are particularly sensitive to anomalous propagation conditions, which can lead to, for example, fluctuations in radar detection ranges or radio signal strengths. Numerous studies have analyzed variations in electromagnetic signals and attributed these changes to atmospheric propagation conditions using, for example, radar (Fornasiero *et al.* 2006, Mesnard and Sauvageot 2010, Magaldi *et al.* 2016), microwave links (Woods *et al.* 2009, Couillard *et al.* 2018, Wang *et al.* 2023), and radio occultation techniques (Kursinski *et al.* 1997, Foelsche *et al.* 2011, Vannah *et al.* 2025).

In the Baltic Sea region, observations of electromagnetic signals have revealed large variability in propagation conditions. Norin (2023) examined six years of clutter in Swedish C-band weather radars originating from coastlines across open water and found a strong seasonal cycle as well as a noticeable diurnal cycle, with clutter being stronger and more frequent during summer and daytime. Rautiainen *et al.* (2025) analyzed two years of data from an X-band coastal radar located on Utö island in the Baltic Sea. They found radar returns from targets at ranges far beyond the normal radar horizon, coinciding with ducting conditions. These observations were most frequent during spring and summer, indicating a seasonal cycle. A similar study was performed by Rautiainen *et al.* (2026) based on one year of Automatic Identification System (AIS) data. Again, a seasonal cycle was found with AIS messages received from far greater distances during spring and summer. These studies demonstrate pronounced seasonal and diurnal variability in propagation conditions across the Baltic Sea region. However, despite the availability of long-term radar and AIS datasets, these provide only indirect and spatially limited insights into atmospheric refractivity.

Another way to examine atmospheric refractivity is through numerical weather prediction (NWP) model data. NWP models provide three-dimensional meteorological fields and can be applied globally or regionally, allowing both spatial and temporal variations in refractivity to be calculated and analyzed. Although NWP models are primarily used for forecasting, reanalysis products allow investigations of historical atmospheric conditions. von Engeln and Teixeira (2004) conducted a global analysis of atmospheric ducts using six years of data based on a combination of reanalysis and operational analysis data from the European Centre for Medium-Range Weather Forecasts (ECMWF) and identified regions with high ducting occurrence. Lopez (2009) extended this work with a five-year global analysis using ECMWF operational analysis data with higher horizontal resolution and a focus on atmospheric ducts closer to the surface. Similar regional studies have been carried out for West Africa (Kaissassou *et al.* 2015, Emmanuel *et al.* 2020, Kaissassou *et al.* 2021), the Black Sea (Sirkova 2015, Feng *et al.* 2025), and the China Seas (Cheng *et al.* 2021, Huang *et al.* 2022, Zhou *et al.* 2022, Yang *et al.* 2023, Liu *et al.* 2024). Zhang *et al.* (2016) used 31 years of data from the National Center for Environmental Prediction Climate Forecast System Reanalysis to study atmospheric ducts in the Gulf of Aden and Wang *et al.* (2025) examined the temporal and spatial characteristics of atmospheric ducts in the Arctic region using a five-year simulation using the Polar WRF model. Despite this growing body of work, no long-term reanalysis-based study of ducting has yet been conducted for the Baltic Sea region.

The availability of high-resolution reanalysis data from 1940 to the present makes it possible to conduct long-term, detailed assessments of atmospheric ducting. In this study, we present a comprehensive analysis of atmospheric ducts over the Baltic Sea region using hourly reanalysis data from 1940 to 2025 to examine their spatial, diurnal, seasonal, and long-term variability.

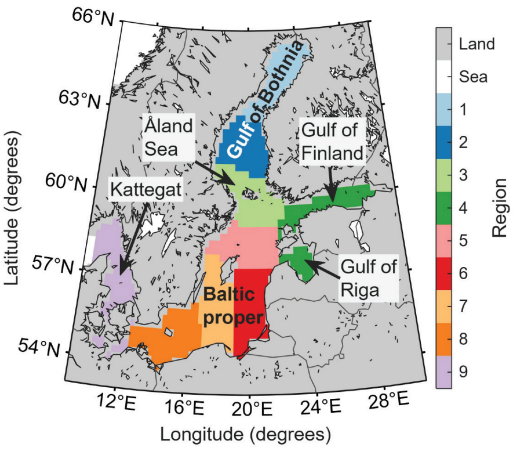

Fig 1. Area selected for the study. Only grid cells with land fraction below 0.25 were included. Land (grey) and inland water bodies (white) were excluded. The study area was subdivided into nine regions for some analyses and visualization.

Data

The fifth generation ECMWF atmospheric reanalysis, ERA5, released in 2016 (Hersbach *et al.* 2020) is a global atmospheric reanalysis that assimilates extensive historical observations with NWP model data to form a consistent, gridded dataset from 1940 to the present. A multi-level ("complete") ERA5 dataset provides meteorological variables on 137 vertical model levels with hourly temporal resolution at a 0.25° spatial grid (Copernicus Climate Change Service 2023a). In addition, a single-level dataset includes near-surface parameters such as 2-m temperature and surface pressure with the same temporal and spatial resolution (Copernicus Climate Change Service 2023b). Together, these datasets allow construction of vertical atmospheric profiles from the surface up to approximately 80 km. In this work, we used both the complete and the single-level datasets. The extracted parameters are listed in Table 1.

The study area covers the Baltic Sea region, extending from 53.5° N, 11° E to 66° N, 29.5° E (Fig. 1). Since this study focuses on marine areas, only grid points with a land fraction less than 0.25 were included in the analysis. For visualization of some analyses, the study area was subdivided into nine regions. The regions were selected to represent both latitudinal and longitudinal variation. Each region consists of 98 grid points, except for region 9, which consists of 99 grid points. All data and analyses are referenced to Coordinated Universal Time (UTC). Local time across the study area ranges from UTC+1 in the west to UTC+2 in the east.

Method

Atmospheric refractivity

The propagation of electromagnetic waves in the atmosphere is governed by spatial variations in the refractive index, n. In the atmosphere, n is very close to unity and it is therefore convenient to define atmospheric refractivity N as $N = (n - 1) \times 10^6$. Using standard meteorological parameters, N can be estimated from the empirical relation (Smith and Weintraub 1953):

$$N = \frac{77.6}{T}\left(p + \frac{4810e}{T}\right), \quad (1)$$

Table 1. ERA5 parameters used in this study. All variables were extracted at hourly resolution.

Parameter	Dataset	Units
2 m air temperature	Single-level	K
2 m dewpoint temperature	Single-level	K
Surface pressure	Single-level	Pa
Land-sea mask	Single-level	
Geopotential	Complete	$m^2\ s^{-2}$
Air temperature	Complete	K
Specific humidity	Complete	$kg\ kg^{-1}$

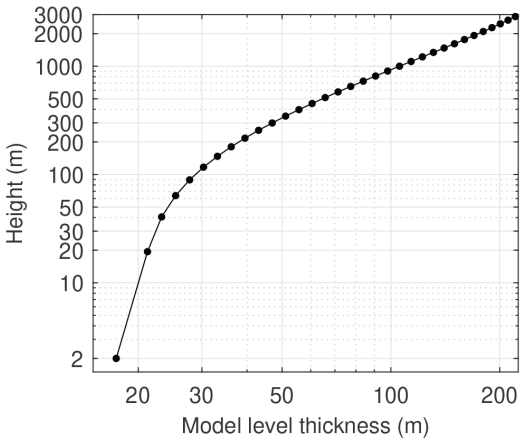

Fig 2. Average height and thickness of model levels in ERA5 in the Baltic Sea region from 1940 to 2025. The exact heights of the model levels depend on the prevailing surface pressure. The standard deviation of the model heights is around 2 %. The level at 2 m originates from ERA5 single level dataset. Figure based on Lopez (2009).

where T is the air temperature (K), p is the atmospheric pressure (hPa), and e is the partial pressure of water vapor (hPa).

To account for the Earth's curvature and facilitate the interpretation of refractive conditions, the modified refractivity M is defined as (Turton *et al.* 1988):

$$M = N + 157H, \tag{2}$$

where H is the height above sea level (km). Using the modified refractivity simplifies the identification of ducting layers in the atmosphere.

Using the ERA5 datasets, we calculated vertical profiles of modified refractivity using Eq. 1 and Eq. 2. Air temperature is provided directly in the ERA5 datasets but the atmospheric pressure, the partial pressure of water vapor, and the geometric height must be derived.

Atmospheric pressure at model levels was derived from model coefficients together with surface pressure and surface geopotential (ECMWF 2024). The geopotential height at model levels was calculated using surface pressure and surface geopotential together with temperature and specific humidity on model levels. Geometric height H was then obtained from geopotential height z using:

$$H = R_e \frac{z}{R_e - z}, \tag{3}$$

where R_e is the Earth's radius at the latitude of interest.

The geometric height at the model levels varies with the prevailing pressure but the lowest model level is typically located at around 20 m above the surface. The average height of model levels up to 3 km and their corresponding thickness (i.e. distance to the next model level) is shown in Fig. 2.

The partial pressure of water vapor, e, can be calculated using (Byers 1974):

$$e = \frac{pq}{0.622 + 0.378q}, \tag{4}$$

where p is the atmospheric pressure in hPa, and q is the specific humidity in kg kg^{-1}.

For the single-level ERA5 dataset, refractivity can be derived using 2 m temperature, surface pressure (which is used to approximate the pressure at 2 m), and the 2 m dewpoint temperature. The partial pressure of water vapor at 2 m can be calculated using the Magnus equation (Lawrence 2005):

$$e = 6.1094 \exp\left(\frac{17.625 T_d}{T_d + 234.04}\right). \tag{5}$$

Here e is the partial pressure of water vapor in hPa and T_d is the dewpoint temperature in °C.

Combining the complete and the single-level ERA5 datasets, hourly vertical profiles of modified refractivity, M, were calculated as a function of geometric height at each grid point in the study area from 1940 to 2025.

Duct properties

Propagation conditions for electromagnetic signals in the atmosphere are determined by the vertical gradient of the modified refractivity, dM/dH. The value of this gradient determines how strongly an electromagnetic signal is refracted. To facilitate interpretation, values of dM/dH are often divided into different propagation regimes (Turton *et al.*, 1988). Normal atmospheric conditions correspond to 79 km^{-1} < dM/dH ≤ 157 km^{-1}. For smaller

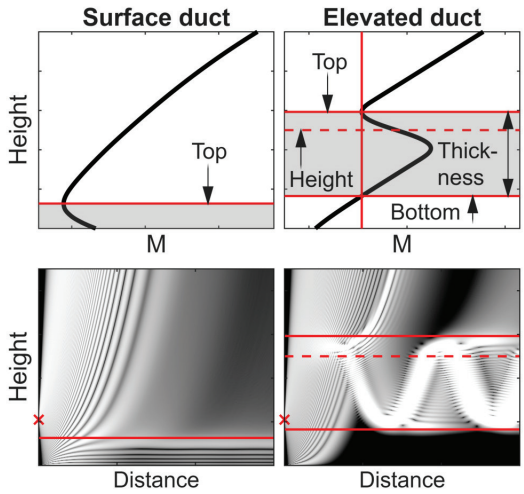

Fig 3. Schematic illustration of two duct types and the corresponding signal propagation behavior. Top row, left: vertical M-profile showing the presence of a surface duct. The surface duct top is defined as the height at which $dM/dH = 0$. Top row, right: An elevated duct occurs when a layer of decreasing refractivity exists at some height. The bottom row shows the propagation factor for a transmitter (located to the left in the figures, marked by a red ×). Bottom row, left: Part of the signal is captured by the surface duct and is guided forward below the duct's top. Bottom row, right: The energy of the signal is captured and guided inside the elevated duct.

values, $0\ \text{km}^{-1} < dM/dH \leq 79\ \text{km}^{-1}$, super-refractive conditions occur, which increasingly bend electromagnetic waves towards the Earth's surface. Ducting, the trapping of electromagnetic waves, occurs when $dM/dH \leq 0\ \text{km}^{-1}$, as the gradient of the atmospheric refractivity fully compensates the Earth's curvature. Sub-refraction, when electromagnetic signals bend less than during normal conditions, occurs when $dM/dH > 157\ \text{km}^{-1}$. The propagation regimes are summarized in Table 2.

A duct thus acts as a layer that traps electromagnetic energy, preventing it from radiating into space and instead guiding it along a specific height. Two distinct types of ducts are commonly described in the literature (see, e.g., Patterson 2008). Surface ducts form close to the sea surface and are often, but not exclusively, caused by a rapid decrease in humidity with height. Ducts can also occur higher in the atmosphere, over both land and sea, and are typically associated with temperature inversions, a rapid decrease in humidity, or both. Such ducts are called elevated ducts, and exist when a local minimum of M occurs at some height above the surface.

The presence of a duct can significantly impact the propagation of electromagnetic signals. Ducts act as waveguides and can trap electromagnetic signals, making them reach longer distances with lower transmission loss than otherwise possible. The two duct types and their characteristic propagation behaviors are illustrated in Fig. 3.

To examine the ERA5 dataset for the presence of ducts, vertical profiles of the modified refractivity were analyzed for every grid point and hour from 1940 to 2025. Profiles were interpolated using cubic splines with approximately 1 m resolution, and the vertical gradient dM/dH was computed starting from the surface upward. The gradient at 10 m was stored as an indicator of near-surface propagation conditions. Because conditions very close to the surface can fluctuate greatly, a surface duct was defined as present whenever $dM/dH < 0$ at 10 m rather than at the surface.

Next, the profiles were examined for surface ducts. If the profile contained a local minimum of M before a local maximum, we recorded a surface duct. By interpolating the M-profile near the local minimum, the height at which $dM/dH = 0$ was calculated, which was defined as the top of the surface duct.

The profiles were then examined for other minima (above any potential surface duct). If such minima were found this indicated the pres-

Table 2. Definitions of atmospheric propagation regimes.

Metric	Ducting	Super refraction	Normal conditions	Sub refraction
dN/dH (km^{-1})	< -157	-157 to -79	-79 to 0	> 0
dM/dH (km^{-1})	< 0	0 to 79	79 to 157	> 157

ence of an elevated duct. Only the lowest such minimum was characterized. The height of the local minimum was defined as the top of the elevated duct whereas the height where dM/dH was smallest was defined as the duct height. The duct bottom was identified as the height at which M was equal to the value of M at the duct top. The thickness of an elevated duct was defined as the difference in height from the duct top to the duct bottom. All duct definitions can be seen in Fig. 3.

The vertical gradient of the modified refractivity, dM/dH consists of five terms (von Engeln and Teixeira 2004):

$$\frac{dM}{dH} = 77.6\frac{dp}{dH}\frac{1}{T} - 77.6\frac{dT}{dH}\frac{p}{T^2} + 3.73\times10^5\frac{de}{dH}\frac{1}{T^2} - 2\times3.73\times10^5\frac{dT}{dH}\frac{e}{T^3} + 157. \quad (6)$$

The first term accounts for the vertical pressure gradient and remains relatively constant. The second term involves the temperature gradient. Because this term has a negative sign, a temperature inversion (i.e. $dT/dH > 0$) contributes to lower values of dM/dH. The third term is proportional to the vertical gradient of water vapor partial pressure, so a decrease in humidity with height therefore leads to lower values of dM/dH. The fourth term is generally smaller than the preceding terms, while the fifth term is a constant.

To obtain a mechanistic understanding of duct formation, we evaluated each term for every grid point and hour at 10 m above the surface, to characterize near-surface conditions, and at the height of an identified elevated duct. When no elevated duct was detected, we set the evaluation height to that of the most recent preceding elevated duct at the same grid point. This approach accounts for the varying heights of elevated ducts while allowing the contributing terms to be compared across different propagation regimes.

Results

Results are presented in two parts: (i) spatial, seasonal, and diurnal patterns of the modified refractivity gradient near the surface together with selected duct properties (height, thickness, and occurrence) for the past 10 years (2016–2025), and (ii) their temporal evolution over the full period (1940–2025). For the past 10 years average values of dM/dH and the selected duct properties are shown to visualize the spatial variation. In order to visualize temporal variations, we chose to divide the Baltic Sea region into nine subregions (Fig. 1). Using these regions, seasonal and diurnal cycles are presented. For the full period, results for each region are shown as time series of the selected duct properties.

Results for the past 10 years (2016–2025)

To analyze spatial variation, we present monthly averages of the selected duct properties for the past 10 years. We further study their seasonal and diurnal variation and visualize these using the nine subregions (cf. Fig. 1).

Spatial variation

The gradient of the modified refractivity, dM/dH, at 10 m above the sea surface provides insight into how atmospheric conditions vary near the surface. Fig. 4 shows the monthly mean values of dM/dH for the period 2016–2025. The mean values of dM/dH clearly vary with both geographic location and season.

During winter (December–February, DJF), conditions are mostly normal except in the eastern Baltic Sea where super-refractive conditions appear. During spring (March–May, MAM), conditions become predominantly super-refractive, and ducting ($dM/dH < 0$) occurs in May in the gulfs of Finland and Riga.

In summer (June–August, JJA), the atmosphere remains mostly super-refractive, except in August in the Gulf of Riga where ducting conditions occur. By autumn (September–November, SON), conditions revert back to normal in the Gulf of Bothnia but remain super-refractive elsewhere.

In this work, a surface duct is considered present if $dM/dH < 0$ at 10 m above the surface. Given that a surface duct exists, it is of interest to

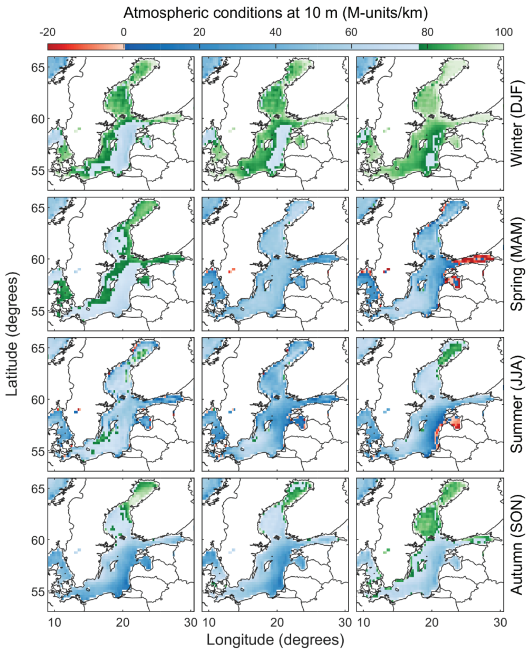

Fig 4. Mean value of the gradient of modified refractivity (*dM*/*dH*) at 10 m above the surface during the period 2016–2025. The 12 panels show the different months. Top row shows winter months, then spring, summer and finally autumn at the bottom. Normal atmospheric conditions are shown in green, super-refractive conditions in blue, and ducting conditions in red.

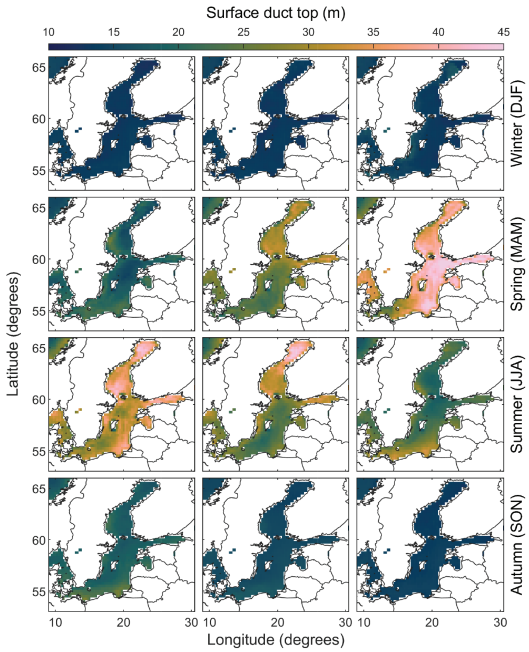

Fig 5. Mean height of surface duct top during the period 2016–2025. Surface ducts are here defined as present if *dM*/*dH* < 0 at 10 m above the surface. Panels arranged as in Fig. 4.

know up to which height it prevails. The average height of surface duct tops is shown in Fig. 5. The mean surface duct top can extend up to about 50 m above the surface, predominantly during May–July in the Baltic proper and the Gulf of Bothnia. During winter and autumn, the mean height of surface duct tops is not much greater than 10 m anywhere in the Baltic Sea region.

The occurrence of surface ducts at 10 m is shown in Fig. 6. Such ducts rarely occur during winter in the Baltic Sea region. In December, surface ducts occur up to 15% of the time in the eastern Baltic proper, elsewhere they are less common. During spring, summer, and autumn, ducting conditions are much more prevalent. In the gulfs of Finland and Riga, surface ducts occur up to 50% of the time during May and August. High occurrence levels, up to 40% of the time, can also be seen in the Kattegat during this period.

The second type of duct examined here is the elevated duct. The mean height at which

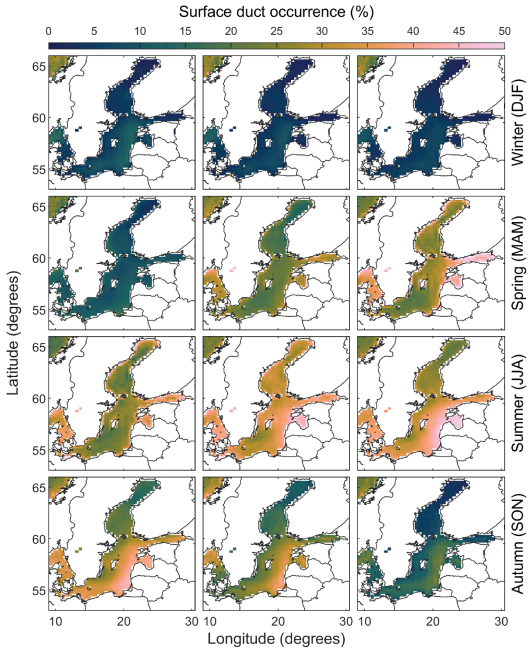

Fig 6. Occurrence of surface ducts during the period 2016–2025. Surface ducts are here defined as present if the value of *dM*/*dH* < 0 at 10 m above the surface. Panels arranged as in Fig. 4.

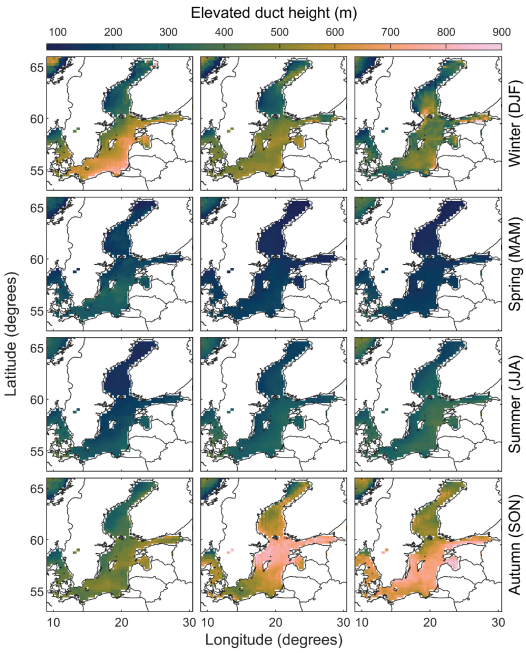

Fig 7. Mean height of elevated ducts during the period 2016–2025. Panels arranged as in Fig. 4.

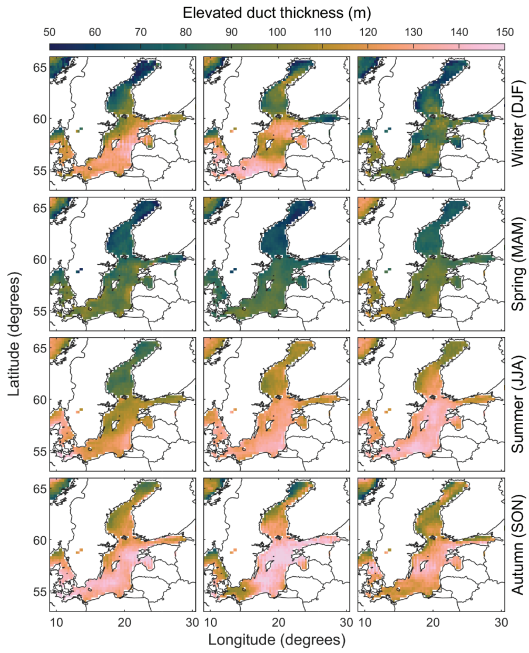

Fig 8. Mean thickness of elevated duct during the period 2016–2025. Panels arranged as in Fig. 4.

elevated ducts can be found is shown in Fig. 7. A strong seasonal cycle can be seen: during spring and summer, the heights of elevated ducts are typically around 100 m to 300 m, whereas during autumn and winter the mean height is larger, extending up to 900 m. The highest ducts are found in the Baltic proper and in the Gulf of Finland during late autumn and early winter.

The mean thickness of elevated ducts is shown in Fig. 8. The mean thickness of elevated ducts is larger in the southern parts of the Baltic Sea region compared to the northern parts. Ducts are generally thickest, up to about 150 m, from July to January. In the Gulf of Bothnia, especially from December to April, the thickness is lower, down to 50 m.

Elevated ducts are most common during the summer, especially in the Baltic proper (Fig. 9). They occur up to 20% of the time during July and August. In the Gulf of Bothnia, they are less common but can occur 10–15% of the time in summer. In late autumn to early spring, October to March, elevated ducts are found less than 5% of the time anywhere in the Baltic Sea region.

Multiple elevated ducts can also occur simultaneously and a surface duct can exist at

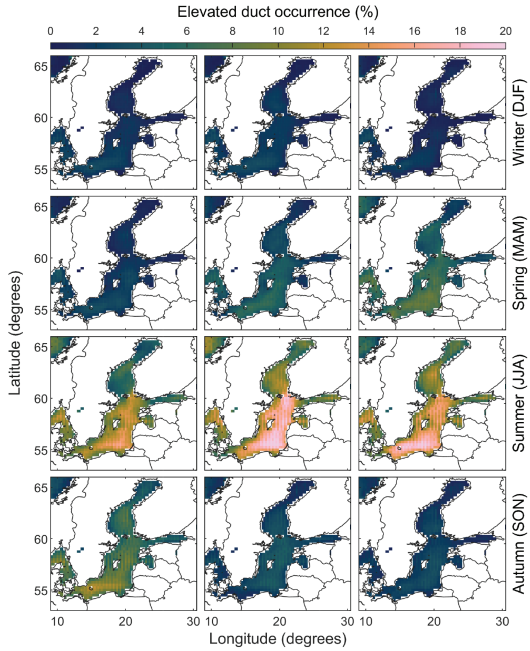

Fig 9. Occurrence of elevated ducts during the period 2016–2025. Panels arranged as in Fig. 4.

the same time and location as an elevated duct. The number of simultaneously existing elevated ducts was counted for all grid points in the study

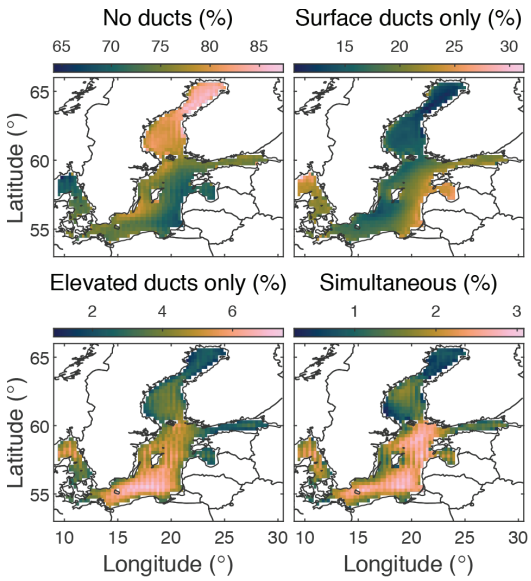

Fig 10. Spatial distribution of the occurrence of no ducts (top left), surface ducts only (top right), elevated ducts only (bottom left), and simultaneous surface and elevated ducts (bottom right) during the period 2016–2025.

area during the period 2016–2025 and was very low. Whenever an elevated duct was present, additional elevated ducts occurred less than 0.33% of the time. Whenever multiple ducts did occur, two simultaneous ducts were found over 99% of the time. Three simultaneous ducts were found in less than 0.03 ‰ of the cases and four simultaneous ducts were only found two times during the entire time period, for all grid points.

Surface ducts can occur simultaneously with elevated ducts, which is a more common phenomenon. Fig. 10 shows the spatial distribution of four separate combinations: no ducts at all, surface ducts only, elevated ducts only, and simultaneous surface and elevated ducts. No ducts is the most common case everywhere in the study area, and is more frequent further north. Surface ducts only is the second most common case, especially along the eastern Baltic coast. Elevated ducts only occur in the Baltic proper and in the Kattegat up to 6% of the time whereas simultaneous ducts occur during less than 3% of the time anywhere. Simultaneous surface and elevated ducts are most prevalent in the Baltic proper and in the Kattegat.

Seasonal and diurnal cycles

Mean values of atmospheric conditions and duct properties do not fully describe when these conditions occur. A complementary way to analyze these metrics is to examine their seasonal and diurnal cycles. Due to the amount of data, it is no longer practical to visualize this information together with the spatial patterns shown above. We therefore make use of the sea regions defined in Fig. 1. Below, we show seasonal and diurnal cycles of dM / dH near the surface together with the selected metrics for the surface and elevated ducts per region.

The top row of Fig. 11 shows dM / dH at 10 m above the surface for the past 10 years as a function of time of year and time of day for the nine different sea regions. All regions display a similar variation, with smaller values of dM / dH during summer and between 10 and 22 UTC. The smallest values of dM / dH, corresponding to ducting conditions, occur in the gulfs of Finland and Riga, the eastern Baltic proper, and the Kattegat (regions 4, 6, and 9), whereas ducting conditions are less often reached in the Gulf of Bothnia (regions 1–2), the Åland Sea (region 3), and the southern and western Baltic proper (regions 7–8).

The height of surface ducts shows a similar variation for all regions (Fig. 11, middle row). During summer nights (around 20 UTC to 05 UTC), surface ducts extend to their largest heights. During winter, surface duct heights barely exceed the required 10 m threshold.

The occurrence of surface ducts has strong seasonal and diurnal cycles (Fig. 11, bottom row). Surface ducts are very common during summer, occurring up to 70% of the time in the gulfs of Finland and Riga (region 4), and are much more common during daytime than at night in all regions.

Elevated duct heights peak during winter (Fig. 12, top row). The diurnal variation is small compared to the seasonal cycle. During winter, elevated ducts are highest in the evening. The seasonal cycle is strong for all regions, with the highest elevated ducts found in the gulfs of Finland and Riga (region 4), the eastern Baltic proper (regions 5–6) and the lowest in the Gulf of Bothnia (regions 1–2) and in the Åland Sea (region 3).

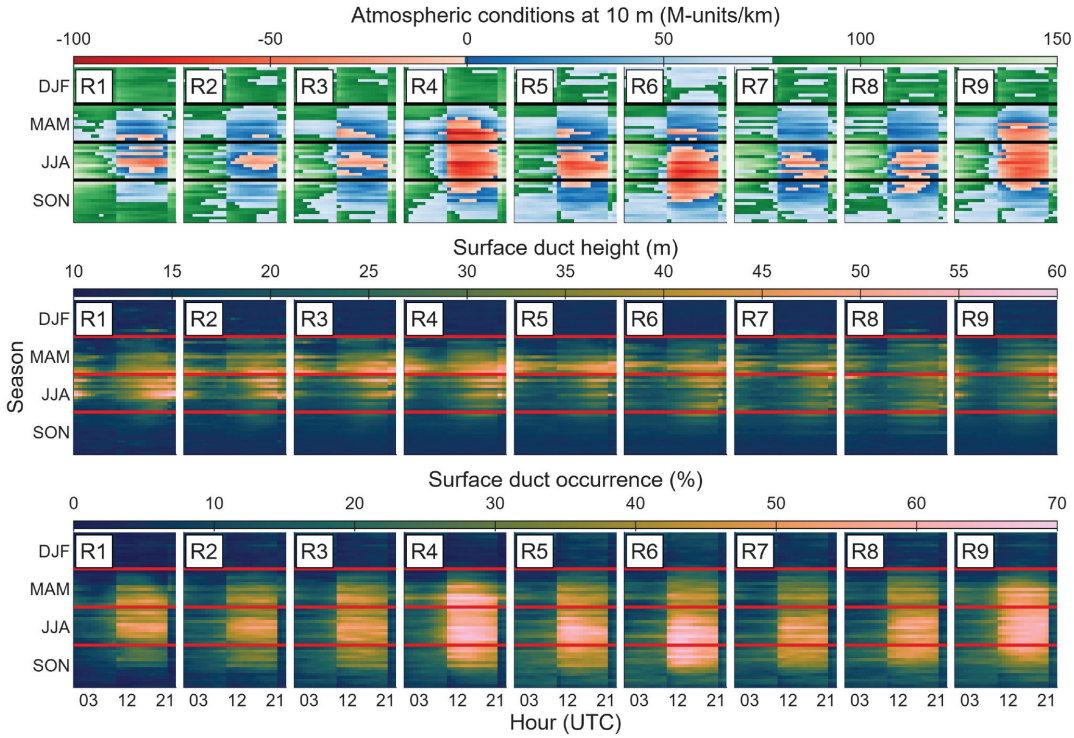

Fig 11. Seasonal and diurnal cycles for surface ducts for the nine sea regions during the period 2016–2025. Top row: Gradient of the modified refractivity (*dM/dH*) at 10 m above the surface. Normal atmospheric conditions are shown in green, super-refractive conditions in blue, and ducting conditions are shown in red. Middle row: Surface duct height. Bottom row: Surface duct occurrence. Black or red horizontal lines mark the start of a new season. R1 means region 1, R2 means region 2, and so on.

The thickness of elevated ducts also displays a more prominent seasonal than diurnal cycle (Fig. 12, middle row). Duct thickness is largest during late summer and autumn in all regions, with the thickest ducts found in the gulfs of Finland and Riga (region 4) and in the Baltic proper (regions 5–8) and the thinnest ducts in the Gulf of Bothnia (regions 1–2) and in the Åland Sea (region 3).

The occurrence of elevated ducts shows both a seasonal and a diurnal component (Fig. 12, bottom row). Elevated ducts are most common during summer and during daytime, occurring more than 25% of the time in the Baltic proper (regions 5–8). During winter, elevated ducts are almost absent in all regions.

As noted above, surface ducts can occur simultaneously with elevated ducts. The seasonal variation of the four combinations (no ducts, surface ducts only, elevated ducts only, and simultaneous surface and elevated ducts) for the nine regions is shown in Fig. 13. The distribution is similar across all regions, with no ducts occurring close to 100% of the time during winter and surface ducts only occurring up to around 30–40% of the time in the summer, especially in the gulfs of Finland and Riga (region 4). Simultaneous ducts are rare but do occur during summer.

Duct formation

The spatial and temporal variations in ducting properties described above can be further interpreted by examining the individual terms contributing to the vertical gradient of modified refractivity, dM / dH.

Empirical cumulative distribution functions (ECDFs) for the first four terms in Eq. (6) at 10 m above the sea surface, separated by season and propagation regime, are presented

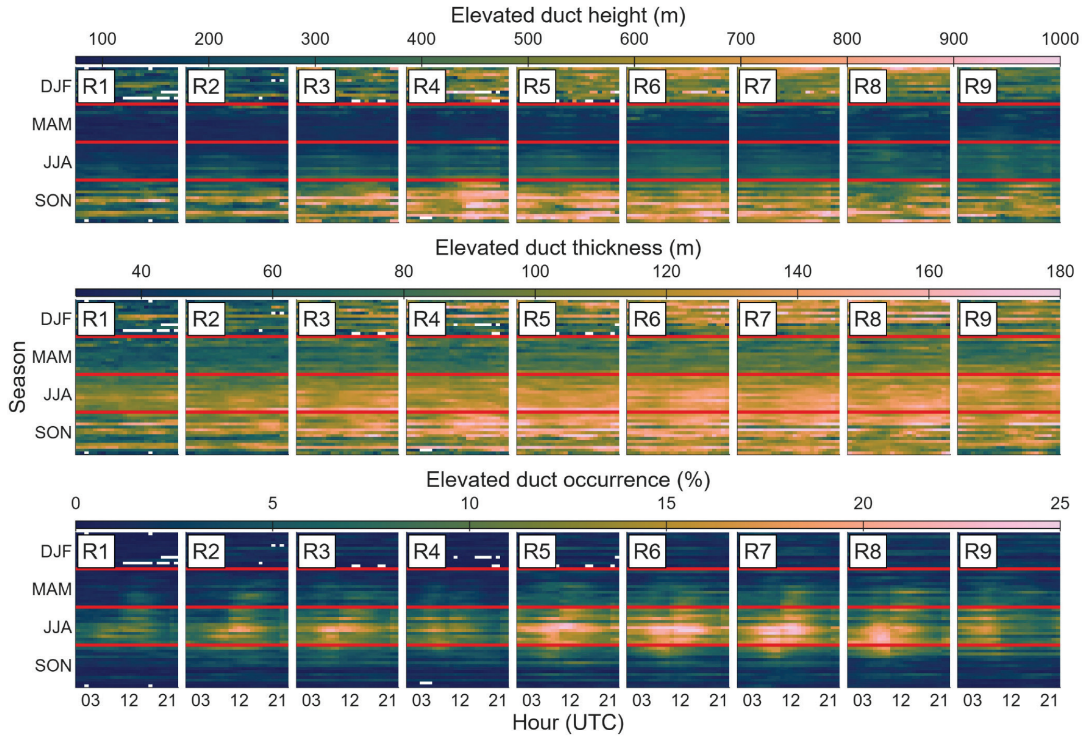

Fig 12. Seasonal and diurnal cycles of elevated ducts for the nine sea regions during the period 2016–2025. Top row: Elevated duct height. Middle row: Elevated duct thickness. Bottom row: Elevated duct occurrence. Red horizontal lines mark the start of a new season. Panels arranged as in Fig. 11.

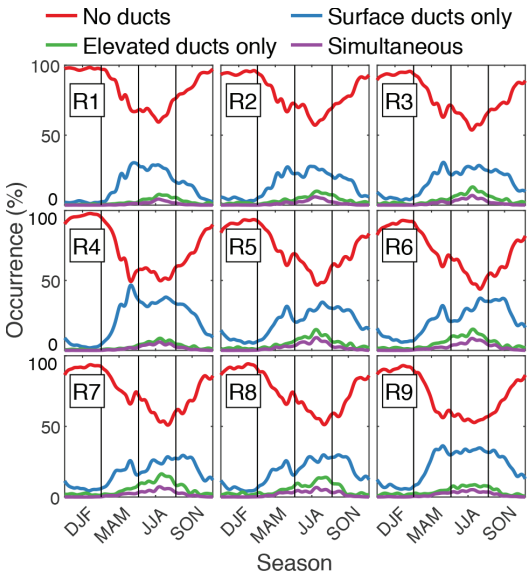

Fig 13. Seasonal cycles of the occurrence during the period 2016–2025 of no ducts, surface ducts only, elevated ducts only, and simultaneous surface and elevated ducts. Black vertical lines mark the start of a new season. R1 means region 1, R2 means region 2, and so on.

in Fig. 14. Term 3, representing the humidity-gradient contribution, shows the clearest separation among the different propagation regimes. Its distributions under ducting conditions are shifted substantially toward negative values, indicating that it is the dominant negative contribution to dM / dH in the near-surface layer. The most negative Term 3 contribution occurs during summer, coinciding with the season of highest surface-duct occurrence. The remaining terms show smaller overall variation, although some seasonal differences are evident, particularly for Terms 2 and 4 under spring ducting conditions. Overall, these distributions suggest that near-surface ducts in the Baltic Sea region are primarily associated with strongly negative humidity-gradient contributions.

The seasonal and diurnal cycles of surface ducts are consistent with enhanced moisture availability near the sea surface during the warm season and daytime. The similar seasonal cycle of the height of the surface-duct top suggests that near-surface humidity gradients may also con-

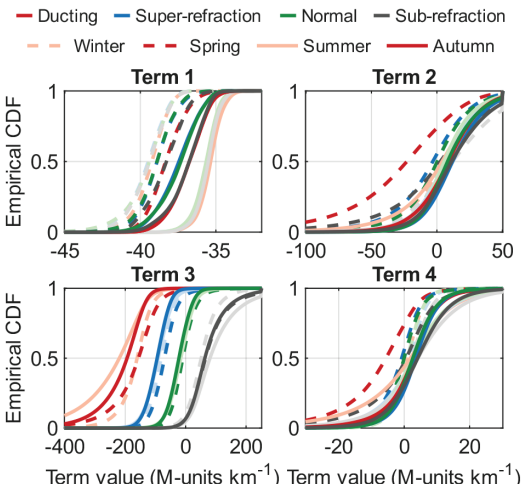

Fig 14. Empirical cumulative distribution functions of the first four terms contributing to *dM/dH* at 10 m above the surface, based on data from 2016–2025. Colors distinguish the propagation regimes, while line styles and shades denote the seasons.

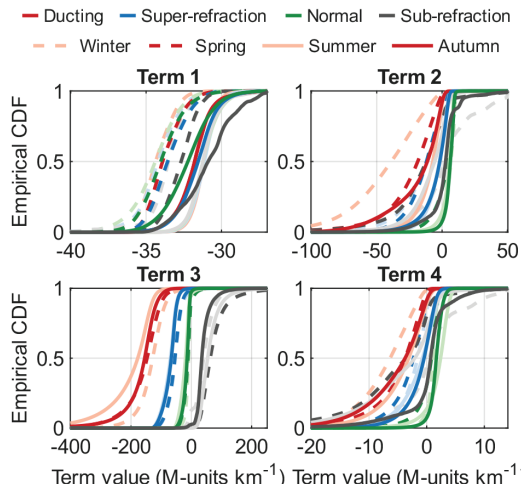

Fig 15. Empirical cumulative distribution functions of the first four terms contributing to *dM/dH* at the height of elevated ducts, based on data from 2016–2025. Colors distinguish the propagation regimes, while line styles and shades denote the seasons.

tribute to variations in duct-top height, although this depends on the complete vertical profile of modified refractivity rather than on the gradient at 10 m alone.

At the heights of elevated ducts, Term 3 remains strongly separated among the propagation regimes, but the temperature-gradient terms (Terms 2 and 4) also exhibit pronounced seasonal differences (Fig. 15). In particular, during winter ducting conditions the distribution of Term 2 is shifted toward more negative values, consistent with the role of temperature inversions in producing elevated ducts during the cold season. During summer, Term 2 is generally less negative, while Term 3 remains important for attaining the ducting threshold. These results suggest that elevated ducting reflects the combined influence of humidity and temperature gradients, with their relative contributions varying seasonally.

Temporal evolution 1940–2025

The results in the previous sections establish the spatial, seasonal, and diurnal patterns of atmospheric and ducting properties during 2016–2025. To place these results in a longer-term context, we compared them with results for the full ERA5 period (1940–2025). Using the same method to calculate the duct metrics, we present the temporal evolution for the nine different sea regions. For each region, season, and metric, a seasonal time series was constructed by calculating one value per year. To enhance visual clarity, the time series shown in Figs. 16–18 were smoothed using a 7-year, Hanning-weighted moving-average filter.

Trends were assessed using the trend-free pre-whitening Mann–Kendall test (Then & Halim, 2026) for the full period (1940–2025) and for the most recent 20-year period (2006–2025). The tests were applied to the original, unsmoothed data, whereas the smoothed time series are used only for visualization. Statistical significance was assessed using two-sided tests at $\alpha = 0.05$. Sen's slope was calculated for each time series and period. Complete results, including the standardized Mann–Kendall statistic, p-value, and Sen's slope, are provided in the Supplementary Information. Table S1 contains the results for surface ducts, Table S2 those for elevated ducts, and Table S3 those for simultaneous ducts. The results discussed below focus on the most relevant statistically significant trends.

The temporal evolution of near-surface atmospheric conditions, surface-duct top height, and surface-duct occurrence by season is shown



Fig 16. Temporal evolution of seasonal means for atmospheric conditions and surface duct properties in the nine sea regions (7-year Hanning-smoothed time series). Top row: Gradient of modified refractivity (*dM/dH*) at 10 m above the sea surface. Middle row: Height of the surface duct top. Bottom row: Surface duct occurrence.

in Fig. 16. Near-surface atmospheric conditions are represented by the mean gradient of modified refractivity, *dM* / *dH*, at 10 m above the surface (Fig. 16, top row).

During winter, *dM* / *dH* remained, on average, between normal and super-refractive conditions, at approximately 80 M-units km^{-1}, throughout the full period. A statistically significant positive trend was detected in all regions except the eastern Baltic proper (region 6). In spring, *dM* / *dH* decreased in all nine regions, from approximately 80 M-units km^{-1} at the beginning of the record to approximately 40 M-units km^{-1} near its end. These decreases were statistically significant over 1940–2025 in all regions. The decline was much steeper during 2006–2025, which is consistent with a more rapid transition toward super-refractive or ducting conditions during spring in recent decades. Summer conditions in 2025 were similar to those in 1940, despite higher *dM* / *dH* values around 2010. Over the full period, statistically significant positive trends occurred in all regions except in the gulfs of Finland and Riga (region 4). In contrast, several regions exhibited statistically significant negative trends during 2006–2025, indicating that the long-term trend was not uniform over time. In autumn, *dM* / *dH* increased in many regions following a shift around 1950. During 2006–2025, however, statistically significant negative trends occurred in several regions, particularly outside the northernmost parts.

The mean surface-duct top height changed little during winter over the full period (Fig. 16, middle row). Although statistically significant trends were detected in some regions during

both analysis periods, their magnitudes were very small and indicate no meaningful change in winter duct-top height. In spring, the surface-duct top height increased significantly over 1940–2025 across all regions, increasing from approximately 18 to 21 m. This long-term increase was not apparent during the most recent 20-year period. During summer, the duct-top height varied considerably, with a mean value of approximately 25 m, but no statistically significant trend was detected in either period. In autumn, the duct-top height was lower, at approximately 15 m, and increased significantly in the southern regions (regions 4–9). This increase was more pronounced during 2006–2025.

Surface-duct occurrence (Fig. 16, bottom row) remained low during winter, generally below 10% throughout the full period. Significant positive trends were detected in most regions during 2006–2025, indicating a recent increase from a low baseline. In spring, occurrence increased significantly in all regions over both the full and recent periods. The stronger recent-period increase is consistent with a seasonal shift toward earlier development of ducting conditions in recent decades. During summer, occurrence remained relatively stable, although statistically significant changes were detected in some regions. The full-period trends were negative in regions 3 and 7–9, including the Kattegat (region 9), where occurrence decreased from above 40% in 1940 to approximately 30% around 2010. In contrast, positive trends were detected in regions 3–6 during 2006–2025, indicating that recent changes did not continue uniformly in the same direction as the long-term trends. In autumn, occurrence was highest in the 1940s and then stabilized near 15% from the 1960s until approximately 2010. The long-term trends were mixed among the regions, whereas positive trends occurred in all regions except furthest to the north (region 1) during 2006–2025. During the past 20 years, the regional differences became more pronounced, with the Gulf of Bothnia (regions 1–2) showing the lowest occurrence, approximately 10–15%, and the eastern Baltic proper (regions 5–6) the highest, approximately 30%.

The temporal evolution of elevated-duct properties is shown in Fig. 17. Elevated-duct heights exhibit distinct regional variations, with the lowest values in the Gulf of Bothnia (regions 1–2) and the highest values in the Baltic proper (regions 5–8). Ducts are highest in winter and autumn, with heights generally ranging from 300 to 600 m. In spring, elevated-duct heights are lowest, ranging from approximately 100 to 250 m, and increase to approximately 200–350 m during summer. In winter, a statistically significant negative trend was only detected for region 1 for the full period but no statistically significant trends were detected during the most recent 20 years. In spring, statistically significant negative trends occurred in regions 3–4 over the full period, whereas a statistically significant positive trend was detected only in region 1 during 2006–2025. In summer, statistically significant positive trends occurred in several regions over the full period, although these trends were not detected during the most recent 20 years. In autumn, statistically significant positive trends were detected in regions 4 and 8 over the full period, while no statistically significant trends were detected during the most recent 20 years.

The thickness of the elevated ducts is shown in Fig. 17 (middle row). The thinnest ducts occur in the Gulf of Bothnia (regions 1–2), whereas the thickest ducts occur in the Baltic proper (regions 5–8). Ducts are generally thickest in summer and thinnest in spring. No significant trends were detected during winter for either period. During the full period, statistically significant positive trends in duct thickness occurred in all regions during both spring and summer. In spring, significant positive trends were also detected in regions 2 and 6 during 2006–2025, whereas only region 1 showed a significant trend during summer. In autumn, a significant positive trend occurred in regions 6–8 over the full period, while no statistically significant trends were detected during the most recent 20 years.

Finally, the bottom row of Fig. 17 illustrates the temporal evolution of elevated-duct occurrence. Occurrence is highest during summer and is generally greater in the southern regions than in the north. No statistically significant trends were detected during winter over the full period and only region 8 showed a significant positive trend during the most recent

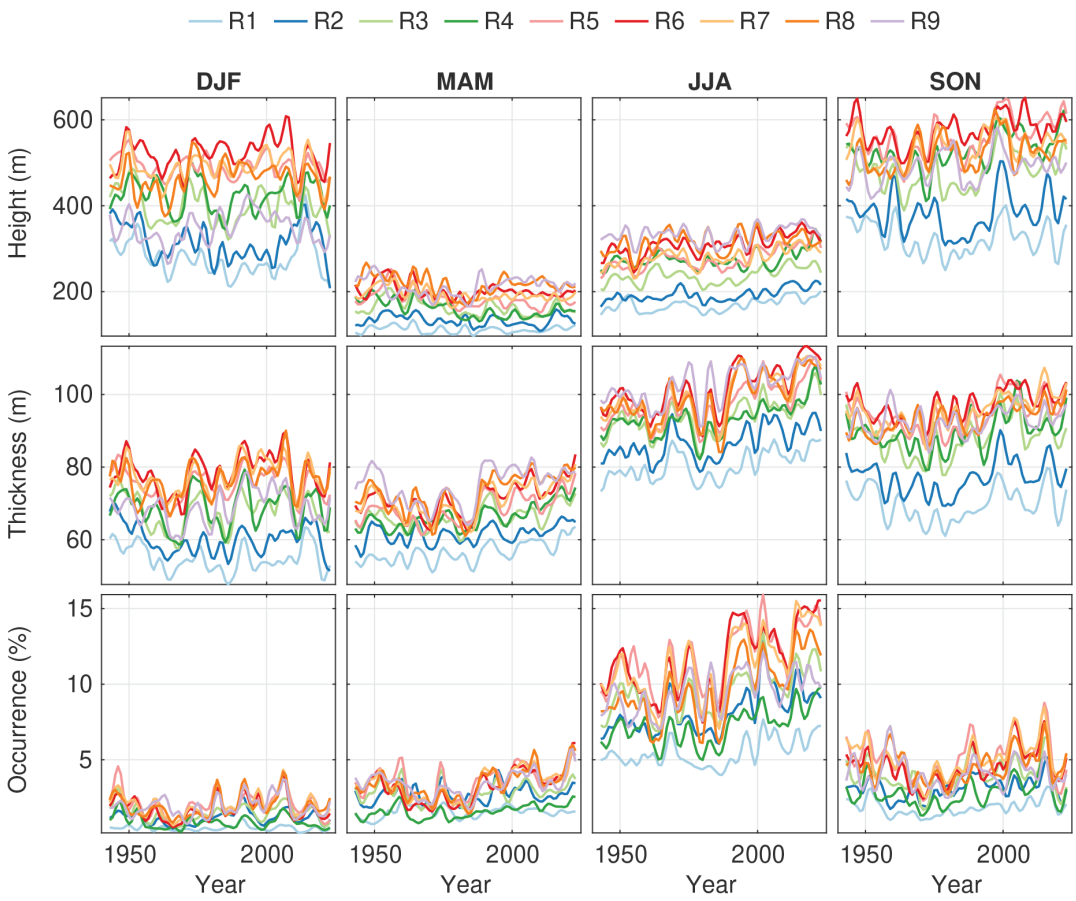

Fig 17. Temporal evolution of seasonal means for elevated ducts in the nine sea regions (7-year Hanning-smoothed time series). Top row: Elevated-duct height. Middle row: Elevated-duct thickness. Bottom row: Elevated-duct occurrence.

20 years. During spring, statistically significant positive trends occurred in regions 4–8 over the full period, although no significant trends were detected during the most recent 20 years. During summer, significant positive trends occurred in all regions over 1940–2025, with additional significant increases in regions 1, 4, and 6 during 2006–2025. No statistically significant trends were detected during autumn.

Ducts can also occur simultaneously. As before, we examine four combinations: no ducts, surface ducts only, elevated ducts only, and simultaneous surface and elevated ducts. The temporal evolution of these cases is shown in Fig. 18. This figure reveals patterns similar to those observed for the past 10 years (cf. Fig. 13): the no-duct condition dominates in all regions and is especially common during winter and autumn. The surface-duct-only condition occasionally reaches 50% occurrence during spring and summer, whereas elevated-duct-only condition is less common (< 25%). Simultaneous surface and elevated ducts occur almost exclusively during spring and summer, and even then, their occurrence rarely exceeds 10%. Only a few statistically significant trends were detected for any combination in any region, and no discernible pattern was found.

Overall, the 1940–2025 time series reveal strong seasonal and regional variability rather than a uniform intensification of ducting conditions. Surface-duct occurrence increased in spring across all regions, consistent with an earlier onset of springtime ducting, and this increase was even stronger during the past 20 years. Elevated-duct height, thickness, and occurrence

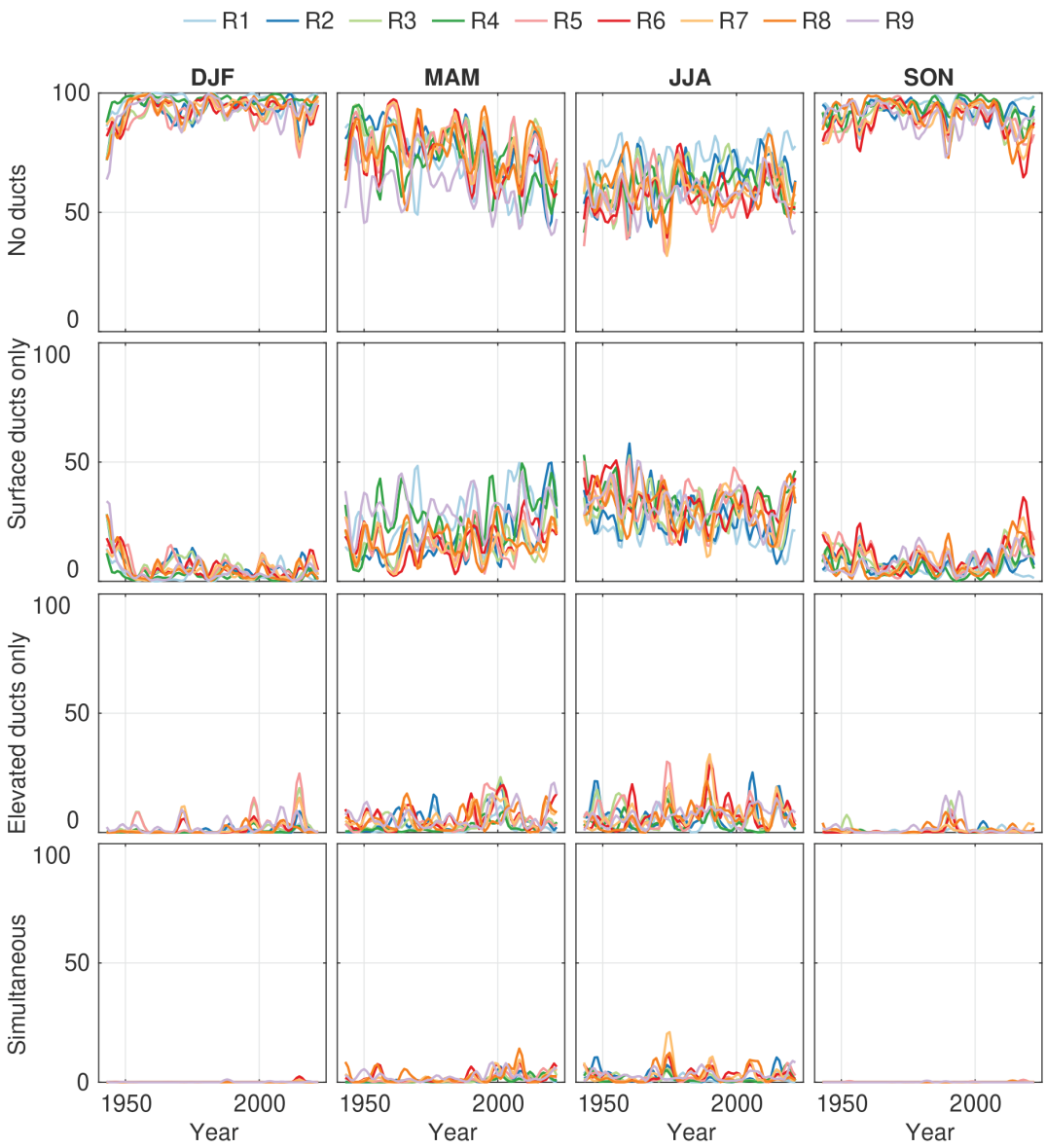

Fig 18. Temporal evolution of seasonal means for duct type combinations in the nine sea regions (7-year Hanning-smoothed time series). Top row: Occurrence of no ducts. Second row: Occurrence of surface ducts only. Third row: Occurrence of elevated ducts only. Bottom row: Occurrence of simultaneous surface and elevated ducts.

increased mainly during spring and summer although trends were generally absent during 2006–2025.

The detected long-term changes and seasonal shifts in ducting conditions can be interpreted in relation to the contributing terms in dM / dH (Figs. 14 and 15). The increase in spring surface-duct occurrence is consistent with a strengthening or earlier development of near-surface humidity gradients. This interpretation is consistent with changes in air–sea moisture exchange that may be driven by the rapid warming of the Baltic Sea surface (Belkin 2009, Dutheil *et al.* 2023, Zalewska *et al.* 2024).

The analysis of the individual terms indicates that humidity gradients are important contributors to both surface ducting and the summer elevated-duct occurrence. Winter elevated-duct

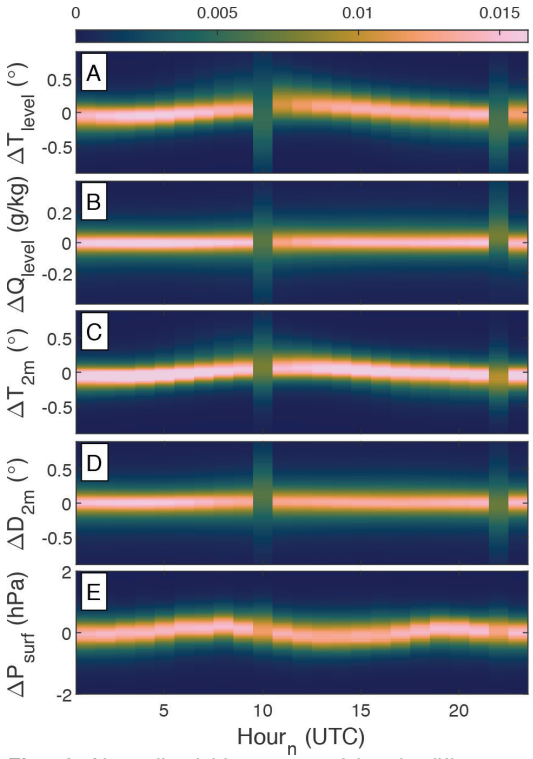

Fig 19. Normalized histograms of hourly differences in selected ERA5 parameters during 2016–2025. For each hour H_n, the difference in parameter values is calculated as H_{n+1}–H_n. (*A*) Temperature at the lowest model level. (B) Specific humidity at the lowest model level. (*C*) Temperature at 2 m. (*D*) Dewpoint temperature at 2 m. (*E*) Surface pressure.

occurrence is more closely associated with temperature inversions and shows no significant long-term trend. These results suggest that the detected changes are more strongly related to moisture-gradient variability during spring and summer than to changes in wintertime thermal stability.

Discussion

The results presented above provide a comprehensive climatology of surface and elevated ducts in the Baltic Sea region based on multi-decadal reanalysis data.

In this study, near-surface atmospheric conditions were evaluated at 10 m above the sea surface. This height is a compromise between the 2 m values available from the ERA5 single-level dataset and the lowest model level in the complete ERA5 dataset, which is usually located at approximately 20 m. Additional analyses using evaluation heights of 15 or 20 m showed the same main spatial, seasonal, and diurnal patterns as the 10 m analysis, although the absolute frequency of detected surface ducts decreased with increasing evaluation height. The variance in the data also decreased with increasing evaluation height because the profiles become increasingly constrained by the model levels. Using a lower evaluation height would instead place more emphasis on the 2 m values, likely resulting in more detected ducts but also leading to greater variability.

Examining duct presence using reanalysis data offers significant benefits but also entails limitations. In this work, only the lowest of the potentially multiple elevated ducts was analyzed. Although simultaneously occurring elevated ducts were found to be rare, this does not imply that multiple elevated ducts are absent in reality, only that they are rarely detected in the ERA5 dataset. As illustrated in Fig. 2, the distance between consecutive model levels increases with height, which may cause the model to miss thinner ducts. This limitation is particularly relevant for elevated ducts at higher altitudes, where vertical resolution is coarser.

The full ERA5 record spans substantial changes in the availability and coverage of observations (Soci *et al.* 2024). The number and geographical coverage of assimilated data were considerably more limited before the expansion of satellite observations in the 1970s. Uncertainty in the dataset is generally greater during the earlier decades and trends over 1940–2025 should therefore be interpreted with caution.

In figures showing the seasonal and diurnal cycles (Figs. 11 and 12), sharp gradients appear around 10–11 UTC and 22–23 UTC. These patterns are not artifacts of data processing but reflect discontinuities in temperature and humidity within the ERA5 dataset. Hourly changes in temperature, specific humidity, and dewpoint temperature were systematically larger at those hours, whereas surface pressure did not exhibit such jumps (Fig. 19). This suggests that the abrupt changes in duct metrics at these times likely reflect model behavior rather than physical

processes, and should therefore be interpreted with caution.

Individual model outputs may contain errors, but the overall spatial and temporal patterns are consistent with available observations in the region. For example, the results show seasonal and diurnal cycles similar to those reported by Norin (2023), Rautiainen *et al.* (2025), and Rautiainen *et al.* (2026). These studies therefore provide qualitative support for the temporal variability identified in this study. A quantitative comparison is not straightforward, however, because radar- and AIS-based observations reflect not only the atmospheric state but also electromagnetic wave propagation, system characteristics, observation geometry, and detection criteria.

This indicates that, despite its limitations, ERA5 provides a valuable dataset for studying the climatology and variability of atmospheric ducting in the Baltic Sea region, although more work is needed to enable quantitative comparisons between reanalysis data and observations. In particular, the observed increase in duct occurrence in recent decades motivates comparisons with long, homogeneous observational records where available.

The forthcoming ERA6 reanalysis (Hersbach 2025) is expected to provide higher spatial resolution and assimilate a broader range of observations, which may improve the representation of fine-scale refractivity structures in future analyses. To explore potential future propagation conditions, complementary studies based on climate model data would also be valuable for assessing how ducting conditions may evolve under future climate scenarios.

Conclusions

The Baltic Sea region is an important area for maritime shipping and has recently also emerged as a geopolitical focal point. In this region, electromagnetic signals are important for communication, navigation and situational awareness. Since atmospheric variations can strongly influence the propagation of electromagnetic signals, understanding atmospheric refractivity in general and atmospheric ducts in particular is of great interest for this region.

In this work, we used the ERA5 reanalysis dataset, which provides meteorological data at hourly temporal and 0.25° spatial resolution from 1940 to 2025, to calculate refractivity and derive the characteristics and occurrence of two duct types: surface ducts and elevated ducts. The analyses focused on examining near-surface refractivity conditions as well as duct properties. Metrics such as height, thickness, and occurrence for two different types of ducts were derived.

The results show strong spatial and temporal variability in atmospheric conditions, with clear seasonal and diurnal cycles. In general, both duct types are more common during summer and daytime and occur more frequently in the southern parts than in the northern parts of the Baltic Sea region. Over the past 20 years, surface-duct occurrence has increased during spring, consistent with a possible shift toward earlier seasonal development.

Given the growing military and geopolitical significance of the Baltic Sea region, improved understanding of spatial and temporal variations in atmospheric propagation conditions is increasingly important. The aim of this work is to contribute to that understanding and provide a foundation for continued investigations. Future work could include comparisons with long, homogeneous observational records to validate and refine the reanalysis-derived duct climatology. Additionally, extending this analysis using climate model projections would help assess how atmospheric ducting conditions may evolve in the coming decades.

Acknowledgements: This work was funded by the Swedish Armed Forces R&D program for Sensors and Signatures (FoT SoS, AT.9220425). The scientific color maps used in this work were created by Crameri (2021) and Brewer (2023).

Supplementary Information: The supplementary information related to this article is available online at: https://doi.org/10.60910/ber2026.5tkp-4036

References

Alappattu D.P., Wang Q. & Kalogiros J. 2016. Anomalous propagation conditions over eastern Pacific Ocean

derived from MAGIC data. Radio Science 51(7): 1142–1156, https://doi.org/10.1002/2016RS005994.

Bean B.R. & Dutton E.J. 1968. Radio meteorology. Dover Publications.

Belkin I.M. 2009. Rapid warming of large marine ecosystems. Progress in Oceanography 81: 207–213, https://doi.org/10.1016/j.pocean.2009.04.011.

Brewer C.A. 2023. Color advice for maps. Penn State [dataset]. Accessed 21 April 2026, https://www.colorbrewer2.org.

Byers H.R. 1974. General meteorology, 4th ed., p. 416. McGraw-Hill.

Cheng Y., Zha M., You Z. & Zhang Y. 2021. Duct climatology over the South China Sea based on European Center for Medium Range Weather Forecast reanalysis data. Journal of Atmospheric and Solar-Terrestrial Physics 222, 105720, https://doi.org/10.1016/j.jastp.2021.105720.

Copernicus Climate Change Service 2023a. Complete ERA5 global atmospheric reanalysis. Copernicus Climate Change Service (C3S) Climate Data Store (CDS). https://doi.org/10.24381/cds.143582cf.

Copernicus Climate Change Service 2023b. ERA5 hourly data on single levels from 1940 to present. Copernicus Climate Change Service (C3S) Climate Data Store (CDS). https://doi.org/10.24381/cds.adbb2d47.

Couillard D., Dahman G., GrandMaison M.-E., Poitau G. & Gagnon F. 2018. Robust broadband maritime communications: theoretical and experimental validation. Radio Science 53(6): 749–760, https://doi.org/10.1029/2018RS006561.

Crameri F. 2021. Scientific colour maps. Zenodo [dataset], version 7.0.1. Accessed 21 April 2026, https://doi.org/10.5281/zenodo.5501399.

Crowther G.A. 2023. The Baltic Sea region at an inflection point. PRISM 10(2): 6–17. https://www.jstor.org/stable/48718170.

Dutheil C., Meier H.E.M., Gröger M. & Börgel F. 2023. Warming of Baltic Sea water masses since 1850. Climate Dynamics 61: 1311–1331, https://doi.org/10.1007/s00382-022-06628-z.

ECMWF 2024. ERA5: compute pressure and geopotential on model levels, geopotential height and geometric height. ECMWF. https://confluence.ecmwf.int/spaces/CKB/pages/158636068/ERA5+compute+pressure+and+geopotential+on+model+levels+geopotential+height+and+geometric+height

Emmanuel I., Ojo O.S., Abe O.E. & Adedayo K.D. 2020. Geostatistical distribution of vertical refractivity gradient over Nigeria. Radio Science 55(9), e2020RS007109, https://doi.org/10.1029/2020RS007109.

von Engeln A. & Teixeira J. 2004. A ducting climatology derived from the European Centre for Medium-Range Weather Forecasts global analysis fields. Journal of Geophysical Research: Atmospheres 109(D18). https://doi.org/10.1029/2003JD004380.

Falodun S.E. & Ajewole M.O. 2006. Radio refractive index in the lowest 100-m layer of the troposphere in Akure, south western Nigeria. Journal of Atmospheric and Solar-Terrestrial Physics 68(2): 236–243, https://doi.org/10.1016/j.jastp.2005.10.002.

Feng C., Wang S., Huang C., Yang F., Shu Y. & Yang K. 2025. Spatial and temporal distributions of evaporation ducts in the Black Sea and their impact on the over-the-horizon propagation of electromagnetic waves. Frontiers in Marine Science 12. https://doi.org/10.3389/fmars.2025.1615118.

Foelsche U., Scherllin-Pirscher B., Ladstädter F., Steiner A.K. & Kirchengast G. 2011. Refractivity and temperature climate records from multiple radio occultation satellites consistent within 0.05%. Atmospheric Measurement Techniques 4: 2007–2018, https://doi.org/10.5194/amt-4-2007-2011.

Fornasiero A., Alberoni P.P. & Bech J. 2006. Statistical analysis and modelling of weather radar beam propagation conditions in the Po Valley (Italy). Natural Hazards and Earth System Sciences 6: 303–314, https://doi.org/10.5194/nhess-6-303-2006.

Grábner M. & Kvičera V. 2003. Refractive index measurement at TV tower Prague. Radioengineering 12(1): 5–7.

Haldén P. (ed.) 2025. The Baltic Sea: a geopolitical history, p. 350. Stolpe Publishing.

HELCOM 2010. Maritime activities in the Baltic Sea – an integrated thematic assessment on maritime activities and response to pollution at sea in the Baltic Sea region. Baltic Sea Environment Proceedings No. 123. Helsinki Commission.

Hersbach H. 2025. From ERA5 to ERA6. European Centre for Medium-Range Weather Forecasts (ECMWF). Presented at the ECMWF User Engagement Forum (UEF 2025). https://events.ecmwf.int/event/464/contributions/5297/attachments/3240/5403/UEF2025_Hersbach.pdf.

Hersbach H., Bell B., Berrisford P., Hirahara S., Horányi A., Muñoz-Sabater J., Nicolas J., Peubey C., Radu R., Schepers D., Simmons A., Soci C., Abdalla S., Abellan X., Balsamo G., Bechtold P., Biavati G., Bidlot J., Bonavita M., De Chiara G., Dahlgren P., Dee D., Diamantakis M., Dragani R., Flemming J., Forbes R., Fuentes M., Geer A., Haimberger L., Healy S., Hogan R.J., Hólm E., Janisková M., Keeley S., Laloyaux P., Lopez P., Lupu C., Radnoti G., de Rosnay P., Rozum I., Vamborg F., Villaume S. & Thépaut J.-N. 2020. The ERA5 global reanalysis. Quarterly Journal of the Royal Meteorological Society 146(730): 1999–2049, https://doi.org/10.1002/qj.3803.

Hou J., Chiao M.-L. & Tsai S. 2024. A case study of offshore evaporation ducts in northeastern Taiwan during summer time. Meteorology and Atmospheric Physics 136, 50, https://doi.org/10.1007/s00703-024-01047-7.

Huang L., Zhao X. & Liu Y. 2022. The statistical characteristics of atmospheric ducts observed over stations in different regions of American mainland based on high-resolution GPS radiosonde soundings. Frontiers in Environmental Science 10. https://doi.org/10.3389/fenvs.2022.946226.

Kaissassou S., Djiotang L., Komkoua A., Ekobo B., Ndzana B., Tanessong R., Guenang M. & Vondou A. 2021. Climatology of super-refraction and trapping layers conditions over Central and West Africa. Meteorologi-

cal Applications 28(4), e2016, https://doi.org/10.1002/met.2016.

Kaissassou S., Lenouo A., Tchawoua C., Lopez P. & Gaye A.T. 2015. Climatology of radar anomalous propagation over West Africa. Journal of Atmospheric and Solar-Terrestrial Physics 123: 1–12, https://doi.org/10.1016/j.jastp.2014.11.009.

Kerr D.E. (ed.) 1987. Propagation of short radio waves. Peter Peregrinus Ltd. on behalf of the IEE.

Kursinski E.R., Hajj G.A., Schofield J.T., Linfield R.P. & Hardesty R.M. 1997. Observing Earth's atmosphere with radio occultation measurements using the Global Positioning System. Journal of Geophysical Research: Atmospheres 102(D19): 23455–23465, https://doi.org/10.1029/97JD01569.

Lawrence M.G. 2005. The relationship between relative humidity and the dewpoint temperature in moist air: a simple conversion and applications. Bulletin of the American Meteorological Society 86(2): 225–234, https://doi.org/10.1175/BAMS-86-2-225.

Liu Q., Zhao X., Zou J., Hu T., Qiu Z., Wang B., Li Z., Cui C. & Cao R. 2024. Investigating the spatio-temporal characteristics of lower atmospheric ducts across the China seas by performing a long-term simulation using the WRF model. Frontiers in Marine Science 11. https://doi.org/10.3389/fmars.2024.1332805.

Lopez P. 2009. A 5-yr 40-km-resolution global climatology of superrefraction for ground-based weather radars. Journal of Applied Meteorology and Climatology 48(1): 89–110, https://doi.org/10.1175/2008JAMC1961.1.

Magaldi A.V., Mateu M., Bech J. & Lorente J. 2016. A long term (1999–2008) study of radar anomalous propagation conditions in the Western Mediterranean. Atmospheric Research 169: 73–85, https://doi.org/10.1016/j.atmosres.2015.09.027.

Mesnard F. & Sauvageot H. 2010. Climatology of anomalous propagation radar echoes in a coastal area. Journal of Applied Meteorology and Climatology 49(11): 2285–2300, https://doi.org/10.1175/2010JAMC2440.1.

Norin L. 2023. Observations of anomalous propagation over waters near Sweden. Atmospheric Measurement Techniques 16(7): 1789–1801, https://doi.org/10.5194/amt-16-1789-2023.

Norin L., Wellander N. & Devasthale A. 2023. Anomalous propagation and the sinking of the Russian warship Moskva. Bulletin of the American Meteorological Society 104(12): E2286–E2304, https://doi.org/10.1175/BAMS-D-23-0113.1.

Østenstad P. & Meltzer M.M. 2023. Measuring refractivity profiles using shipborne unmanned aerial vehicle. OCEANS 2023 – Limerick, 1–6, https://doi.org/10.1109/OCEANSLimerick52467.2023.10244635.

Patterson W.L. 2008. The propagation factor, Fp, in the radar equation. In: Skolnik M.I. (ed.), Radar handbook, 3rd ed., McGraw-Hill, pp. 26-1–26-27.

Rautiainen L., Lensu M., Vakkari V., Tyynelä J., Kanarik H. & Laakso L. 2025. Marine atmospheric ducting statistics based on 2 years of coastal surveillance radar observations. Journal of Applied Meteorology and Climatology 64(1): 63–76, https://doi.org/10.1175/JAMC-D-24-0096.1.

Rautiainen L., Johansson M.M., Lensu M., Tyynelä J., Jalkanen J.-P., Hasu M., Stenbäck K., Lonka H. & Laakso L. 2026. Studying anomalous propagation over marine areas using an experimental AIS receiver set-up. Atmospheric Measurement Techniques 19(8): 2763–2785, https://doi.org/10.5194/amt-19-2763-2026.

Sirkova I. 2015. Duct occurrence and characteristics for Bulgarian Black Sea shore derived from ECMWF data. Journal of Atmospheric and Solar-Terrestrial Physics 135: 107–117, https://doi.org/10.1016/j.jastp.2015.10.017.

Smith E.K. & Weintraub S. 1953. The constants in the equation for atmospheric refractive index at radio frequencies. Journal of Research of the National Bureau of Standards 50(1): 39–41, https://doi.org/10.6028/JRES.050.006.

Steiner M. & Smith J.A. 2002. Use of three-dimensional reflectivity structure for automated detection and removal of nonprecipitating echoes in radar data. Journal of Atmospheric and Oceanic Technology 19(5): 673–686, https://doi.org/10.1175/1520-0426(2002)019<0673:UOTDRS>2.0.CO;2.

Swistek G. & Paul M. 2023. Geopolitics in the Baltic Sea region: the "Zeitenwende" in the context of critical maritime infrastructure, escalation threats and the German willingness to lead. SWP Comment 2023/C 09, Stiftung Wissenschaft und Politik (SWP) – German Institute for International and Security Affairs. https://doi.org/10.18449/2023C09.

Soci C., Hersbach H., Simmons A., Poli P., Bell B., Berrisford P., Horányi A., Muñoz-Sabater J., Nicolas J., Radu R., Schepers D., Villaume S., Haimberger L., Woollen J., Buontempo C. & Thépaut J.-N. 2024. The ERA5 global reanalysis from 1940 to 2022. Quarterly Journal of the Royal Meteorological Society 150(764): 4014–4048, https://doi.org/10.1002/qj.4803.

Then Y.J. & Abdul Halim S. 2026. Modified Mann-Kendall with higher-order statistics for trend analysis. Scientific Reports 16, 500, https://doi.org/10.1038/s41598-025-30034-0.

Turton J.D., Bennetts D.A. & Farmer S.F.G. 1988. An introduction to radio ducting. Meteorological Magazine 117(1393): 245–254.

Vannah S., Leroy S.S., Ao C.O., Kursinski E.R., Nelson K.J., Wang K.-N. & Xie F. 2025. The impact of differences in retrieval algorithms between processing centers on GNSS radio occultation refractivity retrievals in the planetary boundary layer. Atmospheric Measurement Techniques 18: 4293–4310, https://doi.org/10.5194/amt-18-4293-2025.

Wang J., Zhao X., Zou J., Yang P., Wang B., Yang S., Qiu Z., Li Z., Hu T. & Song M. 2025. Investigating the temporal and spatial characteristics of lower atmospheric ducts in the Arctic via long-term numerical simulations. Atmosphere 16(1), 11, https://doi.org/10.3390/atmos16010011.

Wang S., Yang K., Shi Y., Zhang H., Yang F., Hu D., Dong G. & Shu Y. 2023. Long-term over-the-horizon microwave channel measurements and statistical analysis in evaporation ducts over the Yellow Sea.

Frontiers in Marine Science 10. https://doi.org/10.3389/fmars.2023.1077470.

Woods G.S., Ruxton A., Huddlestone-Holmes C. & Gigan G. 2009. High-capacity, long-range, over ocean microwave link using the evaporation duct. IEEE Journal of Oceanic Engineering 34(3): 323–330, https://doi.org/10.1109/JOE.2009.2020851.

Yang N., Su D. & Wang T. 2023. Atmospheric ducts and their electromagnetic propagation characteristics in the northwestern South China Sea. Remote Sensing 15(13), 3317, https://doi.org/10.3390/rs15133317.

Zalewska T., Wilman B., Łapeta B., Marosz M., Biernacik D., Wochna A., Saniewski M., Grajewska A. & Iwaniak M. 2024. Seawater temperature changes in the southern Baltic Sea (1959–2019) forced by climate change. Oceanologia 66(1): 37–55, https://doi.org/10.1016/j.oceano.2023.08.001.

Zhang Q., Yang K. & Shi Y. 2016. Spatial and temporal variability of the evaporation duct in the Gulf of Aden. Tellus A: Dynamic Meteorology and Oceanography 68(1). https://doi.org/10.3402/tellusa.v68.29792.

Zhou Y., Liu Y., Qiao J., Li J. & Zhou C. 2022. Statistical analysis of the spatiotemporal distribution of lower atmospheric ducts over the seas adjacent to China, based on the ECMWF reanalysis dataset. Remote Sensing 14(19). https://doi.org/10.3390/rs14194864.